ARTICLE

Tunable, Strain-Controlled Nanoporous MoS₂ Filter for Water Desalination

Weifeng Li,[†] Yanmei Yang,[†] Jeffrey K. Weber,[‡] Gang Zhang,*[,§] and Ruhong Zhou*[,†,‡,∥]

[†]School for Radiological and Interdisciplinary Sciences (RAD-X) and Collaborative Innovation Center of Radiation Medicine of Jiangsu Higher Education Institutions, Soochow University, Suzhou 215123, China
[‡]Computational Biological Center, IBM Thomas J. Watson Research Center, Yorktown Heights, New York 10598, United States
[§]Institute of High Performance Computing, A*STAR, 138632 Singapore
[∥]Department of Chemistry, Columbia University, New York, New York 10027, United States

S *Supporting Information*

ABSTRACT: The deteriorating state of global fresh water resources represents one of the most serious challenges that scientists and policymakers currently face. Desalination technologies, which are designed to extract potable water from the planet's bountiful stores of seawater, could serve to alleviate much of the stress that presently plagues fresh water supplies. In recent decades, desalination methods have improved via water-filtering architectures based on nanoporous graphene filters and artificial membranes integrated with biological water channels. Here, we report the auspicious performance (in simulations) of an alternative nanoporous desalination filter constructed from a MoS₂ nanosheet. In striking contrast to graphene-based filters, we find that the "open" and "closed" states of the MoS₂ filter can be regulated by the introduction of mechanical strain, yielding a highly tunable nanopore interface. By applying lateral strain to the MoS₂ filter in our simulations, we see that the transition point between "open" and "closed" states occurs under tension that induces about 6% cross-sectional expansion in the membrane (6% strain); the open state of the MoS₂ filter demonstrates high water transparency and a strong salt filtering capability even under 12% strain. Our results thus demonstrate the promise of a controllable nanoporous MoS₂ desalination filter, wherein the morphology and size of the central nanopore can be precisely regulated by tensile strain. These findings support the design and proliferation of tunable nanodevices for filtration and other applications.

KEYWORDS: *MoS₂, water desalination, nanopore, strain control, tunable nanodevice, molecular dynamics*
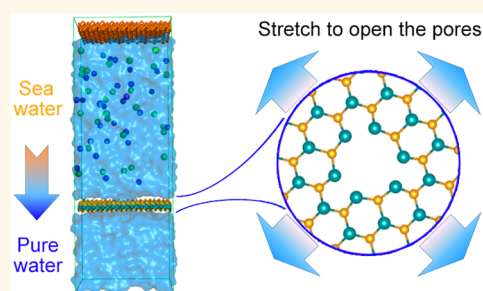
T he confluence of population growth, rapid urban development, and global climate change has stressed available freshwater resources throughout the world.[1] Seawater, which exists in profoundly large supply, represents a plentiful resource from which potable water reserves might be augmented, provided that existing technological hurdles can be overcome. Naturally, the utility of transforming seawater into freshwater relies on the implementation of practical desalination technologies on a large scale. For the past half-century, the most prevalent desalination method has been reverse osmosis (RO).[2] In RO, a semipermeable membrane is placed at the interface between seawater and pure water; pressure is then applied at the seawater side to facilitate the flow of water through the ion-exclusive membrane.

Thanks to advances in nanotechnology, novel approaches for membrane design based on two-dimensional (2D) nanomaterials have greatly improved filter technology in recent years. One particular graphene-derived nanoporous filter, which was first proposed by computer simulations[3−6] and recently realized in experiments,[7,8] represents a milestone in desalination nanotechnology. The advantages of this graphene filter are derived from its exceptional thinness (featuring only one atomic layer), its high mechanical stability, and the simple techniques by which nanosized pores can be introduced into graphene sheets (either through ionic irradiation or chemical treatment). These precisely sized nanopores allow water molecules or certain kinds of ions to pass through the graphene filter and block the flux of other components in the solvent.[7]

In addition to graphene, many other mono- or few-layered 2D materials—like hexagonal boron nitride,[9] silicene,[10,11] phosphorene,[12−15] and molybdenum disulfide (MoS₂)[16]—have been created. Among them, MoS₂ (for which a monolayer form was first synthesized by chemical exfoliation in 2011) has demonstrated unique electronic and optical properties that have encouraged its application in an array of nano-technologies.[16−25] MoS₂ is thermally and mechanically stable,
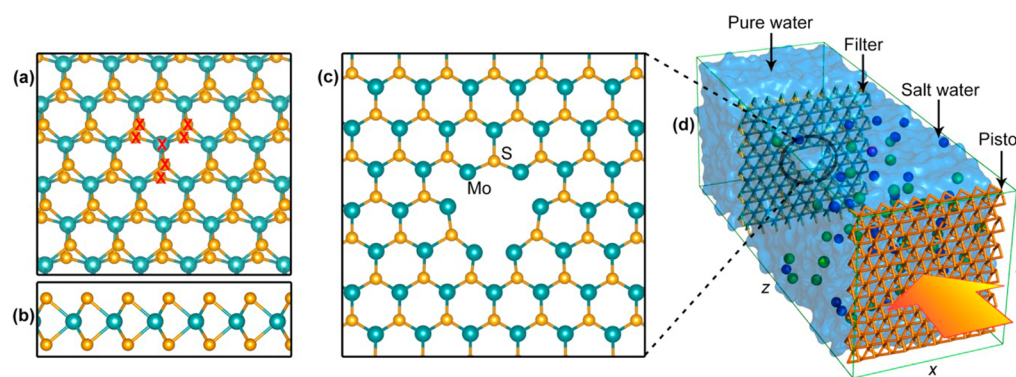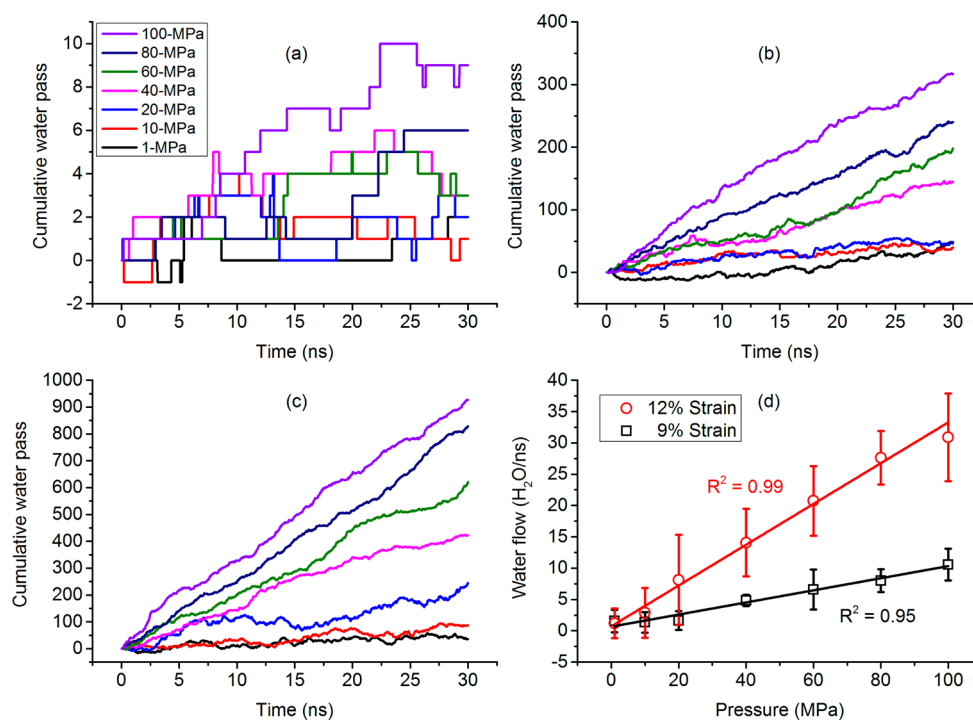
Figure 1. (a) Bird's-eye view and (b) side view of a MoS$_2$ monolayer. Atoms labeled with red crosses are removed to generate the nanopore. (c) Top view of the modeled MoS$_2$ nanopore. (d) Illustration of the simulation model.

Figure 2. Cumulative water flux through the MoS$_2$ filter under piston pressures ranging from 1 to 100 MPa. Here, the MoS$_2$ filter is under respective tensile strains of (a) 6%, (b) 9%, and (c) 12%. (d) Dependence of water flow with respect to pressure at strain levels of 9% and 12%.

featuring a melting point reaching 1185 °C. In chemistry, MoS$_2$-derived materials are used as hydrogen evolution catalysts,[26,27] hydrogen storage media,[28] and functional materials created through surface conjugation or coating.[29−32] Vacancies can be easily introduced into the MoS$_2$ monolayer during chemical vapor deposition,[33,34] suggesting that nanoporous MoS$_2$ can be used in water desalination applications. Importantly, due to the sandwich-like structure of the MoS$_2$ monolayer, its Young's modulus (∼270 GPa) is significantly smaller than that of graphene (∼1 TPa).[35] A MoS$_2$ nanofilter should thus be sensitive to mechanical strain, meaning its exclusion capabilities could be regulated through the application of tensile force. Such tunability would prove very useful for designing controllable nanodevices that could filter water under various conditions and efficiency constraints. Another unique property of MoS$_2$ over the well-studied graphene is the electron redistribution between Mo and S atoms that is absent in graphene, of which all the C atoms are neutral. As a consequence, when nanopores are introduced in

MoS$_2$ filter, the nanopore edge atoms are intrinsically charged. Such charged pore edges have been demonstrated to be important to alter the ion selectivity and water permeability.[3]

In this work, we employ molecular dynamics simulations to evaluate the performance of a MoS$_2$-based filter for seawater desalination. We find that the "open" and "closed" states of the filter are, in fact, easily controlled via the application of tensile strain; the transition point between the two states is observed at about 6% cross-sectional expansion (i.e., 6% strain). We demonstrate that this MoS$_2$ filter has high water transparency and a vigorous salt filtering capability, efficiently blocking the flow of Na$^+$ and Cl$^−$ ions up to 12% strain; potentials of mean force reveal distinct filtering mechanisms for Na$^+$ and Cl$^−$ ions. We discuss the details of our calculations, and the implications they hold for novel desalination nanotechnologies, in depth below.
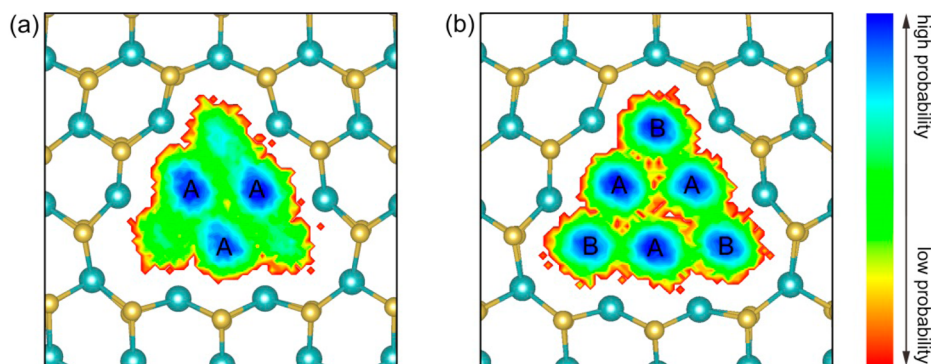
Figure 3. Water flux projected onto the cross section of the MoS$_2$ nanopore when placed under strain levels of (a) 9% and (b) 12%.

RESULTS AND DISCUSSION

The structure of the MoS$_2$ monolayer is illustrated in Figure 1a and b. On the basis of the top view, it is evident that MoS$_2$ shares the hexagonal lattice structure of graphene. Each Mo atom in the central sublayer is covalently bound to six S atoms; S atoms are arranged into two sublayers, forming the sandwich architecture shown in Figure 1b. The atoms highlighted by red crosses in Figure 1a are removed to generate the nanoporous MoS$_2$ layer shown in Figure 1c. Similar vacancy defects have previously been reported in experiments.[33] Our first simulation model is illustrated in Figure 1d: the water box is separated into two regions by a nanopore-containing MoS$_2$ filter. One region of the water box contains NaCl to mimic seawater, whereas the other side is comprised of pure water. A piston (composed of an unperforated MoS$_2$ monolayer) is placed between the saltwater and pure water compartments. In our simulations, force was applied on the piston (at 1, 10, 20, 40, 60, 80, and 100 MPa pressure equivalents) in the z direction to encourage the water flow toward the pure water compartment. Strain on the MoS$_2$ filter was modulated by increasing and fixing the size of its cross-sectional area in the x−y plane. Below, we consider strain magnitudes corresponding to 0%, 3%, 6%, 9%, and 12% cross-sectional area increases.

Under unstrained and mildly strained (3%) conditions, no water passage through the MoS$_2$ filter was observed over the full range of pressures tested, indicating that the MoS$_2$ filter is closed in the absence of sufficient strain. The transition point from "closed" to "open" appears at a strain level near 6%: as illustrated in Figure 2a, a small amount of water does pass through the 6% strained MoS$_2$ filter when pressure is applied. The scale of fluctuations at the 6% strain level is quite large, however, and the expected dependence of water flux on the piston pressure is correspondingly weak. At larger strain magnitudes of 9% (Figure 2b) and 12% (Figure 2c), the MoS$_2$ filter becomes more transparent to water, and the flux of water increases almost linearly with respect to the piston pressure (Figure 2d). We estimated the water permeability of the filter by calculating the slope in Figure 2d. For MoS$_2$ filter under a strain of 12%, the permeability is 1.0×10^{-15} g s^{-1} atm^{-1} per pore. From the experiment, the concentration of intrinsic defects in MoS$_2$ samples reaches 10^{13} cm^{-2}.[36,37] Assuming a nanopore density of 1.0×10^{13} cm^{-2} after re-engineering, the water permeability of the MoS$_2$ filter reaches roughly 100 g m^{-2} s^{-1} atm^{-1}. This is compatible with that measured experimentally for the graphene filter ($\sim$70 g m^{-2} s^{-1} atm^{-1}) under similar condition.[8] We note that, by a precise treatment of the MoS$_2$ monolayer, a higher concentration of the pore may be introduced. The actual water filtering

performance of a MoS$_2$ filter is expected to be higher as the water permeability will scale linearly with the pore density. For the comparison, the performance of commercial RO membrane is usually on the order of 0.1 L cm^{-2} day^{-1} MPa^{-1} (1.18 g m^{-2} s^{-1} atm^{-1}).[3] Thus, MoS$_2$ filter has a potential to achieve a water permeability of 2 orders of magnitude higher than the commercial RO.

These findings suggest that our MoS$_2$ filter can be effectively tuned via mechanical stretching; this property might be leveraged in the future to create a controllable nanodevice that dictates solute/solvent transduction according to nanopore size. It needs to be noted that rare Cl$^-$ transduction events begin to occur under extreme strain and pressure conditions: one chloride ion slipped through the 12%-strained MoS$_2$ filter at both 10 and 100 MPa pressures (see Figure S1). Encouragingly, no Na$^+$ ions passed through the nanopore in any of our simulations. Such observations suggest that the filter, in practice, could operate successfully under tension levels between 9% and 12%. Once calibrated, this strained MoS$_2$ filter thus demonstrates high water transparency and an exceptional salt filtering capability, two features requisite of an effective desalination device.

To quantitatively compare the effect of filter strain on water passage, we have calculated the water flux projected onto the cross section of the MoS$_2$ filter under strain levels of 9% (Figure 3a) and 12% (Figure 3b). Under 9% strain, three flow channels (the areas labeled with "A" in Figure 3a) for water transduction appear near the centers of the edges that define the nanopore triangle. When the strain is increased to 12%, three additional flow channels emerge (labeled with "B" in Figure 3b) at the corners of the nanopore triangle. It seems, therefore, that the tension-based control of the MoS$_2$ filter can simply be attributed to the structural changes of the nanopore that occur under tensile strain: stretching enlarges the nanopore, effectively decreasing the steric hindrance on water flux (the applied pressure also has some effects on the structural deformation of the MoS$_2$ membrane and nanopore, see Figure S2, but in general, these effects are small and negligible in our current settings).

The gate-opening effect has actually been previously implied in organic layered materials, in particular, flexible porous coordination polymers (PCPs) and metal−organic frameworks (MOFs).[38−43] These frameworks can change from a closed structure to an open one during the adsorption/coordination process (especially for gaseous adsorption) at a specific pressure. Such a structural dynamism is identified as a key principle for high selectivity, accommodation, and molecular sensing.[44−46]
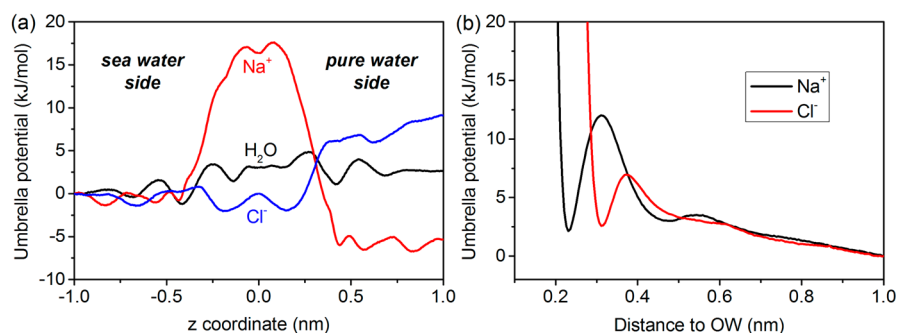
Figure 4. (a) Nonequilibrium potentials of mean force (NPMFs) for water (black), Na$^+$ (red), and Cl$^-$ (blue) across a 12% strained MoS$_2$ nanopore separating seawater from pure water. (b) Free energy profiles for a water molecule to escape the solvation shells of Na$^+$ (black) and Cl$^-$ (red) ions. The x axis is the distance between an ion and water oxygen (OW).

To probe the physical forces governing this MoS$_2$ filter's operation, we have computed—using umbrella sampling techniques—nonequilibrium potentials of mean force (NPMFs) for water molecules, Na$^+$, and Cl$^-$ passing through the MoS$_2$ nanopore interface. Here, we focus our simulations on piston-relaxed "filtration" conditions, wherein the perforated nanolayer separates saltwater from pure water and no piston pressure is applied. As the filter is permeable to all solution components (albeit to a limited extent), its equilibrium state features equal salt concentrations on both sides of the nanosheet. The PMF associated with this nonequilibrium state, therefore, should not be interpreted as a free energy. Rather, the curves in Figure 4a describe the average forces experienced by water molecules and ions over the series of filtration-relevant configurations accessed in simulations. Because salt translocation occurs on exceptionally long time scales, we have also calculated equilibrium PMFs (which can rigorously be interpreted as free energy profiles) for a nanopore systems prepared with equal saltwater concentrations on both sides of the MoS$_2$ membrane (see Figure S4).

As shown in Figure 4a, the NPMF for water is largely diffusive, featuring no energy barrier or well exceeding 5 kJ/mol in absolute value. Water can thus pass through the nanopore with relative ease, explaining the high water permeability of the filter noted in pressure-driven simulations. By contrast, Na$^+$ ions face a very high energetic barrier (on the order of ~20 kJ/mol) upon approaching the nanopore from either side, ensuring that such cations are effectively filtered. This high barrier to Na$^+$ translocation can likely be attributed to two main physical characteristics of the system. First, and perhaps most importantly, the Mo atoms at the extreme nanopore edge are positively charged as six neutralizing sulfur atoms were removed to create the pore opening. The filter interface thus presents a high Coulombic barrier to cationic passage. Second, the steric exclusion effects of the nanopore disfavor Na$^+$ translocation in particular. To pass through the narrow center of the filter, ions must be stripped of their solvation shells. Though Na$^+$ has a smaller radius than Cl$^-$, water molecules in Na$^+$'s first solvation shell are more tightly bound than those associated with Cl$^-$ ions. Figure 4b validates this statement: the free energy barrier to extracting a water molecule from the hydration shell of a Na$^+$ ion (9.90 kJ/mol) is more than twice as high as that of Cl$^-$ (4.36 kJ/mol). As a consequence, the average water exchange time (WET) for Na$^+$ is calculated to be 27.22 ± 0.26 ps, while it is only 8.58 ± 0.03 ps for Cl$^-$.

Similar (but symmetric) barriers to sodium translocation appear in the Na$^+$ equilibrium PMF (see Figure S4). The

apparent low energy "plateau" on the freshwater side of the Na$^+$ NPMF largely arises from electrostatic screening differences unique to the nonequilibrium system (Figure 4a). During the approach of Na$^+$ ions from the left side of the filter (saltwater to freshwater), repulsive interactions with pore's Mo atoms are screened by Cl$^-$ counterions, reducing the total height of the barrier as compared to that from the right side (which has no chloride counterion screening), thus a lower energy plateau on the freshwater side. The ionic strength difference between the freshwater and saltwater sides and the entropic force driving the equalization of salt concentrations also likely contribute to the appearance of the freshwater Na$^+$ basin to a small extent.

The filtration mechanism for Cl$^-$ ions contrasts sharply with that observed for Na$^+$. Two small energy wells appear symmetrically distributed right around the nanopore center (|z| < ~0.25 nm) in the NPMF, suggesting that Cl$^-$ ions should accumulate around the nanopore entrance. This observation is perhaps expected, given the partial positive charges on the Mo atoms at the extreme nanopore edge. Similar wells appear in the Cl$^-$ equilibrium PMF (Figure S4). Nonequilibrium effects, however, also contribute to the monolayer's Cl$^-$ filtration capability. The plateau that emerges on the freshwater side of the Cl$^-$ NPMF can again be attributed to nonequilibrium electrostatic screening: from the right, chloride's attraction to the nanopore center is not tempered by the presence of sodium binding partners, leading to a precipitous decline in the Cl$^-$ NPMF upon approach. A moderate energy barrier (of ~9 kJ/mol) thus appears that impedes Cl$^-$ passage through the nanopore interface in the filtration direction. Notably, this total barrier to Cl$^-$ filter escape is about half of that corresponding to Na$^+$, perhaps explaining why only Cl$^-$ transduction events (though very limited) were seen under 12% strain and high piston pressures (where the NPMF is further tilted toward the freshwater side).

Notably, replicating the force-response properties of transition metal complexes (like the MoS$_2$ nanosheets studied here) is a notoriously difficult proposition from the perspective of classical MD simulations. In light of this fact, we have also performed first-principles calculations on our MoS$_2$ nanosheet to validate the open-pore structures generated by the classical force field. Structural optimizations suggest that, at the level of strain applied in this work, the open-pore configurations observed in our dynamical simulations (at 12% strain) are indeed structurally stable. At higher levels of strain (e.g., 15%), however, coordination changes in pore-edge Mo atoms begin to occur (see Figure S5), suggesting our present model breaks

down when tensile strain increases beyond the limits tested in this work.

For MoS$_2$ monolayer, there exists several types of intrinsic defects as resolved by STEM.[33] The vacancy defect studied in the current work has the largest size. For other types of defects, their size is too narrow to pass water as revealed from our trial calculations. Thus, MoS$_2$ monolayers with intrinsic defects is a reasonable starting place for water permeability and salt rejection. To enhance the performance, achieving controllable pores is desirable. Nanopores with desired diameter can be introduced into 2D materials in a controllable manner. Taking the well-studied graphene, for example, point defects are first introduced into the graphene lattice through ion bombardment and subsequently enlarged by oxidative etching into permeable pores. The pore size can be tuned by controlling the oxidation time. This capability has been successfully demonstrated for the preparation of graphene filter in a recent experiment.[7] For MoS$_2$, point defects can also be introduced through ion bombardment.[47] That said, controlled generation of permeable pores into MoS$_2$ does require additional experimental capability in design and fabrication.

In addition, for the applying of strain to MoS$_2$ filter, several types of experimental works have provided approaches: (1) Gerd Plechinger et al. demonstrated a way to apply biaxial tensile strain to single-layer MoS$_2$ by profiting from the large mismatch between the thermal expansion coefficients of MoS$_2$ and a polydimethylsiloxane (PDMS) substrate.[48] (2) In the second approach by He et al., monolayered MoS$_2$ was deposited directly on poly(methyl methacrylate) (PMMA) substrate. Strain was applied to the substrate to induce bending of PMMA and accordingly the stretching of MoS$_2$.[49]

Other than this, porous piezoelectric substrate (quartz) has also been adopted to control the size of nanopore using biasing voltage across the substrate.[50] First, laser excitation was adopted to generate pores in the quartz whose sizes can be fine-tuned from hundreds of nanometers to tens of micrometers. Biasing voltage was then applied on the porous quartz, which can significantly enlarge the pore size through piezoelectric deformation. Hence, stacking of MoS$_2$ samples onto the porous quartz substrate is possible, which provides the necessary support and controllable tensile stresses, and thus deserves further research efforts in the future.

CONCLUSION

In this work, albeit through a very simple filter model, we have successfully designed a nanopore with "open" and "closed" states by which water flow and ion filtering can be regulated. Mechanical stretching of the filter effectively changes the size of its nanopore and stimulates the passage of water; both steric and electrostatic effects contribute to block the concomitant passage of ions. In these regards, the filter studied above is biomimetic: perforated MoS$_2$ monolayers featuring a selection of functional characteristics that have evolved in biological desalination filters. The performance of this de novo designed filter, however, should benefit from the stability of inorganic molybdenum nanomaterials and relative ease of strain-based control. Though the experimental realization of MoS$_2$ nanofilters will require some additional effort in design and fabrication, the auspicious performance of the MoS$_2$ desalination filter reported in this study certainly justifies further investigation.

METHODS

All the molecular dynamics simulations were carried out using the GROMACS package.[51] The all-atom CHARMM force field was used for Na$^+$ and Cl$^-$ ions, and the TIP3P water model[52] was adopted for the explicit solvent. For MoS$_2$, the force field developed by V. Varshney et al. was used, which has been well documented to reproduce the crystal strusture and experimental vibrational spectra of MoS$_2$.[53] SHAKE constraints[54] were applied to all bonds involving hydrogen atoms. The long-range electrostatic interactions were treated with the particle mesh Ewald method,[55,56] and a typical distance cutoff of 12 Å was used for the van der Waals interactions. The nonbonded interaction pair list was updated every 10 fs. The cross section in the $x-y$ plane of the simulation box was fixed to a certain value in order to place strain on the MoS$_2$ filter. Canonical sampling was performed through the velocity rescaling method[57] at constant temperature of 300 K. An integration time step of 1 fs was used in all simulations.

The simulation box (as illustrated in Figure 1d) contains 3000 water molecules, 30 Na$^+$, 30 Cl$^-$, a MoS$_2$ filter, and an ideal MoS$_2$ monolayer used as a piston. For each strain percentage, the system was first equalibrated with z-direction pressure coupling at 1 atm for 10 ns, followed by 30 ns productive simulations under a given constant piston pressure in the otherwise NVT ensemble.

ASSOCIATED CONTENT

Ⓢ Supporting Information

The Supporting Information is available free of charge on the ACS Publications website at DOI: 10.1021/acsnano.5b05250.

Further details and discussions on the two chloride translocation events, gate size and deformation under pressure, calculations of 2D-projected water flux and potential of mean force, and first-principles calculations to check the structural stability of MoS$_2$ filter under strain. (PDF)

AUTHOR INFORMATION

Corresponding Authors
*E-mail: zhangg@ihpc.a-star.edu.sg (G.Z.).
*E-mail: ruhongz@us.ibm.com (R.H.Z.).

Notes
The authors declare no competing financial interest.

REFERENCES

(1) Elimelech, M.; Phillip, W. A. The Future of Seawater Desalination: Energy, Technology, and the Environment. *Science* **2011**, *333*, 712−717.

(2) Sidney, L.; Srinivasa, S. Sea Water Demineralization by Means of an Osmotic Membrane. In *Saline Water Conversion II*; American Chemical Society: Washington, DC, 1963; Vol. 38, pp 117−132.

(3) Cohen-Tanugi, D.; Grossman, J. C. Water Desalination across Nanoporous Graphene. *Nano Lett.* **2012**, *12*, 3602−3608.

(4) Sint, K.; Wang, B.; Král, P. Selective Ion Passage through Functionalized Graphene Nanopores. *J. Am. Chem. Soc.* **2008**, *130*, 16448−16449.

(5) Suk, M. E.; Aluru, N. Water Transport through Ultrathin Graphene. *J. Phys. Chem. Lett.* **2010**, *1*, 1590−1594.

(6) Sun, C.; Boutilier, M. S.; Au, H.; Poesio, P.; Bai, B.; Karnik, R.; Hadjiconstantinou, N. G. Mechanisms of Molecular Permeation

through Nanoporous Graphene Membranes. *Langmuir* **2014**, *30*, 675−682.

(7) O'Hern, S. C.; Boutilier, M. S.; Idrobo, J.-C.; Song, Y.; Kong, J.; Laoui, T.; Atieh, M.; Karnik, R. Selective Ionic Transport through Tunable Subnanometer Pores in Single-Layer Graphene Membranes. *Nano Lett.* **2014**, *14*, 1234−1241.

(8) Surwade, S. P.; Smirnov, S. N.; Vlassiouk, I. V.; Unocic, R. R.; Veith, G. M.; Dai, S.; Mahurin, S. M. Water Desalination Using Nanoporous Single-Layer Graphene. *Nat. Nanotechnol.* **2015**, *10*, 459−464.

(9) Watanabe, K.; Taniguchi, T.; Kanda, H. Direct-Bandgap Properties and Evidence for Ultraviolet Lasing of Hexagonal Boron Nitride Single Crystal. *Nat. Mater.* **2004**, *3*, 404−409.

(10) Lalmi, B.; Oughaddou, H.; Enriquez, H.; Kara, A.; Vizzini, S.; Ealet, B.; Aufray, B. Epitaxial Growth of a Silicene Sheet. *Appl. Phys. Lett.* **2010**, *97*, 223109.

(11) Vogt, P.; De Padova, P.; Quaresima, C.; Avila, J.; Frantzeskakis, E.; Asensio, M. C.; Resta, A.; Ealet, B.; Le Lay, G. Silicene: Compelling Experimental Evidence for Graphenelike Two-Dimensional Silicon. *Phys. Rev. Lett.* **2012**, *108*, 155501.

(12) Liu, H.; Neal, A. T.; Zhu, Z.; Luo, Z.; Xu, X.; Tománek, D.; Ye, P. D. Phosphorene: An Unexplored 2D Semiconductor with a High Hole Mobility. *ACS Nano* **2014**, *8*, 4033−4041.

(13) Reich, E. S. Phosphorene Excites Materials Scientists. *Nature* **2014**, *506*, 19−19.

(14) Li, W.; Zhang, G.; Zhang, Y.-W. Electronic Properties of Edge-Hydrogenated Phosphorene Nanoribbons: A First-Principles Study. *J. Phys. Chem. C* **2014**, *118*, 22368−22372.

(15) Li, W.; Yang, Y.; Zhang, G.; Zhang, Y.-W. Ultrafast and Directional Diffusion of Lithium in Phosphorene for High-Performance Lithium-Ion Battery. *Nano Lett.* **2015**, *15*, 1691−1697.

(16) Coleman, J. N.; Lotya, M.; O'Neill, A.; Bergin, S. D.; King, P. J.; Khan, U.; Young, K.; Gaucher, A.; De, S.; Smith, R. J.; et al. Two-Dimensional Nanosheets Produced by Liquid Exfoliation of Layered Materials. *Science* **2011**, *331*, 568−571.

(17) Wang, Z.; Li, H.; Liu, Z.; Shi, Z.; Lu, J.; Suenaga, K.; Joung, S.-K.; Okazaki, T.; Gu, Z.; Zhou, J.; et al. Mixed Low-Dimensional Nanomaterial: 2D Ultranarrow MoS$_2$ Inorganic Nanoribbons Encapsulated in Quasi-1D Carbon Nanotubes. *J. Am. Chem. Soc.* **2010**, *132*, 13840−13847.

(18) Radisavljevic, B.; Radenovic, A.; Brivio, J.; Giacometti, V.; Kis, A. Single-Layer MoS$_2$ Transistors. *Nat. Nanotechnol.* **2011**, *6*, 147−150.

(19) Wang, Q. H.; Kalantar-Zadeh, K.; Kis, A.; Coleman, J. N.; Strano, M. S. Electronics and Optoelectronics of Two-Dimensional Transition Metal Dichalcogenides. *Nat. Nanotechnol.* **2012**, *7*, 699−712.

(20) Chhowalla, M.; Shin, H. S.; Eda, G.; Li, L.-J.; Loh, K. P.; Zhang, H. The Chemistry of Two-Dimensional Layered Transition Metal Dichalcogenide Nanosheets. *Nat. Chem.* **2013**, *5*, 263−275.

(21) Wang, X.; Feng, H.; Wu, Y.; Jiao, L. Controlled Synthesis of Highly Crystalline MoS$_2$ Flakes by Chemical Vapor Deposition. *J. Am. Chem. Soc.* **2013**, *135*, 5304−5307.

(22) Li, W.; Zhang, G.; Guo, M.; Zhang, Y.-W. Strain-Tunable Electronic and Transport Properties of MoS$_2$ Nanotubes. *Nano Res.* **2014**, *7*, 518−527.

(23) Cai, Y.; Zhang, G.; Zhang, Y.-W. Polarity-Reversed Robust Carrier Mobility in Monolayer MoS$_2$ Nanoribbons. *J. Am. Chem. Soc.* **2014**, *136*, 6269−6275.

(24) Cui, X.; Lee, G.-H.; Kim, Y. D.; Arefe, G.; Huang, P. Y.; Lee, C.-H.; Chenet, D. A.; Zhang, X.; Wang, L.; Ye, F.; et al. Multi-Terminal Transport Measurements of MoS$_2$ Using a Van Der Waals Heterostructure Device Platform. *Nat. Nanotechnol.* **2015**, *10*, 534−540.

(25) Li, W.; Guo, M.; Zhang, G.; Zhang, Y.-W. Edge-Specific Au/Ag Functionalization-Induced Conductive Paths in Armchair MoS$_2$ Nanoribbons. *Chem. Mater.* **2014**, *26*, 5625−5631.

(26) Hinnemann, B.; Moses, P. G.; Bonde, J.; Jørgensen, K. P.; Nielsen, J. H.; Horch, S.; Chorkendorff, I.; Nørskov, J. K. Biomimetic Hydrogen Evolution: MoS$_2$ Nanoparticles as Catalyst for Hydrogen Evolution. *J. Am. Chem. Soc.* **2005**, *127*, 5308−5309.

(27) Li, Y.; Wang, H.; Xie, L.; Liang, Y.; Hong, G.; Dai, H. MoS$_2$ Nanoparticles Grown on Graphene: An Advanced Catalyst for the Hydrogen Evolution Reaction. *J. Am. Chem. Soc.* **2011**, *133*, 7296−7299.

(28) Chen, J.; Kuriyama, N.; Yuan, H.; Takeshita, H. T.; Sakai, T. Electrochemical Hydrogen Storage in MoS$_2$ Nanotubes. *J. Am. Chem. Soc.* **2001**, *123*, 11813−11814.

(29) Chou, S. S.; De, M.; Kim, J.; Byun, S.; Dykstra, C.; Yu, J.; Huang, J.; Dravid, V. P. Ligand Conjugation of Chemically Exfoliated MoS$_2$. *J. Am. Chem. Soc.* **2013**, *135*, 4584−4587.

(30) Chou, S. S.; Huang, Y.-K.; Kim, J.; Kaehr, B.; Foley, B. M.; Lu, P.; Dykstra, C.; Hopkins, P. E.; Brinker, C. J.; Huang, J.; et al. Controlling the Metal to Semiconductor Transition of MoS$_2$ and WS$_2$ in Solution. *J. Am. Chem. Soc.* **2015**, *137*, 1742−1745.

(31) Zhu, C.; Zeng, Z.; Li, H.; Li, F.; Fan, C.; Zhang, H. Single-Layer MoS$_2$-Based Nanoprobes for Homogeneous Detection of Biomolecules. *J. Am. Chem. Soc.* **2013**, *135*, 5998−6001.

(32) Kiriya, D.; Tosun, M.; Zhao, P.; Kang, J. S.; Javey, A. Air-Stable Surface Charge Transfer Doping of MoS$_2$ by Benzyl Viologen. *J. Am. Chem. Soc.* **2014**, *136*, 7853−7856.

(33) Zhou, W.; Zou, X.; Najmaei, S.; Liu, Z.; Shi, Y.; Kong, J.; Lou, J.; Ajayan, P. M.; Yakobson, B. I.; Idrobo, J.-C. Intrinsic Structural Defects in Monolayer Molybdenum Disulfide. *Nano Lett.* **2013**, *13*, 2615−2622.

(34) Yu, Z.; Pan, Y.; Shen, Y.; Wang, Z.; Ong, Z.-Y.; Xu, T.; Xin, R.; Pan, L.; Wang, B.; Sun, L.; et al. Towards Intrinsic Charge Transport in Monolayer Molybdenum Disulfide by Defect and Interface Engineering. *Nat. Commun.* **2014**, *5*, 5290.

(35) Bertolazzi, S.; Brivio, J.; Kis, A. Stretching and Breaking of Ultrathin MoS$_2$. *ACS Nano* **2011**, *5*, 9703−9709.

(36) Qiu, H.; Xu, T.; Wang, Z.; Ren, W.; Nan, H.; Ni, Z.; Chen, Q.; Yuan, S.; Miao, F.; Song, F.; et al. Hopping Transport through Defect-Induced Localized States in Molybdenum Disulphide. *Nat. Commun.* **2013**, *4*, 2642.

(37) Hong, J.; Hu, Z.; Probert, M.; Li, K.; Lv, D.; Yang, X.; Gu, L.; Mao, N.; Feng, Q.; Xie, L.; et al. Exploring Atomic Defects in Molybdenum Disulphide Monolayers. *Nat. Commun.* **2015**, *6*, 6293.

(38) Kitagawa, S.; Kondo, M. Functional Micropore Chemistry of Crystalline Metal Complex-Assembled Compounds. *Bull. Chem. Soc. Jpn.* **1998**, *71*, 1739−1753.

(39) Kitagawa, S.; Kitaura, R.; Noro, S. i. Functional Porous Coordination Polymers. *Angew. Chem., Int. Ed.* **2004**, *43*, 2334−2375.

(40) Bradshaw, D.; Warren, J. E.; Rosseinsky, M. J. Reversible Concerted Ligand Substitution at Alternating Metal Sites in an Extended Solid. *Science* **2007**, *315*, 977−980.

(41) Serre, C.; Mellot-Draznieks, C.; Surblé, S.; Audebrand, N.; Filinchuk, Y.; Férey, G. Role of Solvent-Host Interactions That Lead to Very Large Swelling of Hybrid Frameworks. *Science* **2007**, *315*, 1828−1831.

(42) Tanaka, D.; Nakagawa, K.; Higuchi, M.; Horike, S.; Kubota, Y.; Kobayashi, T. C.; Takata, M.; Kitagawa, S. Kinetic Gate−Opening Process in a Flexible Porous Coordination Polymer. *Angew. Chem.* **2008**, *120*, 3978−3982.

(43) Nijem, N.; Wu, H.; Canepa, P.; Marti, A.; Balkus, K. J., Jr; Thonhauser, T.; Li, J.; Chabal, Y. J. Tuning the Gate Opening Pressure of Metal−Organic Frameworks (MOFs) for the Selective Separation of Hydrocarbons. *J. Am. Chem. Soc.* **2012**, *134*, 15201−15204.

(44) Halder, G. J.; Kepert, C. J.; Moubaraki, B.; Murray, K. S.; Cashion, J. D. Guest-Dependent Spin Crossover in a Nanoporous Molecular Framework Material. *Science* **2002**, *298*, 1762−1765.

(45) Kubota, Y.; Takata, M.; Matsuda, R.; Kitaura, R.; Kitagawa, S.; Kobayashi, T. C. Metastable Sorption State of a Metal−Organic Porous Material Determined by in Situ Synchrotron Powder Diffraction. *Angew. Chem., Int. Ed.* **2006**, *45*, 4932−4936.

(46) Hijikata, Y.; Horike, S.; Sugimoto, M.; Inukai, M.; Fukushima, T.; Kitagawa, S. Pore Design of Two-Dimensional Coordination

Polymers toward Selective Adsorption. *Inorg. Chem.* **2013**, *52*, 3634–3642.

(47) Inoue, A.; Komori, T.; Shudo, K.-i. Atomic-Scale Structures and Electronic States of Defects on Ar$^+$-Ion Irradiated MoS$_2$. *J. Electron Spectrosc. Relat. Phenom.* **2013**, *189*, 11–18.

(48) Plechinger, G.; Castellanos-Gomez, A.; Buscema, M.; van der Zant, H. S.; Steele, G. A.; Kuc, A.; Heine, T.; Schüller, C.; Korn, T. Control of Biaxial Strain in Single-Layer Molybdenite Using Local Thermal Expansion of the Substrate. *2D Mater.* **2015**, *2*, 015006.

(49) He, K.; Poole, C.; Mak, K. F.; Shan, J. Experimental Demonstration of Continuous Electronic Structure Tuning *via* Strain in Atomically Thin MoS$_2$. *Nano Lett.* **2013**, *13*, 2931–2936.

(50) Stava, E.; Yu, M.; Shin, H. C.; Shin, H.; Kreft, D. J.; Blick, R. H. Rapid Fabrication and Piezoelectric Tuning of Micro-and Nanopores in Single Crystal Quartz. *Lab Chip* **2013**, *13*, 156–160.

(51) Van Der Spoel, D.; Lindahl, E.; Hess, B.; Groenhof, G.; Mark, A. E.; Berendsen, H. J. C. Gromacs: Fast, Flexible, and Free. *J. Comput. Chem.* **2005**, *26*, 1701–1718.

(52) Jorgensen, W. L.; Chandrasekhar, J.; Madura, J. D.; Impey, R. W.; Klein, M. L. Comparison of Simple Potential Functions for Simulating Liquid Water. *J. Chem. Phys.* **1983**, *79*, 926–935.

(53) Varshney, V.; Patnaik, S. S.; Muratore, C.; Roy, A. K.; Voevodin, A. A.; Farmer, B. L. MD Simulations of Molybdenum Disulphide (MoS$_2$): Force-Field Parameterization and Thermal Transport Behavior. *Comput. Mater. Sci.* **2010**, *48*, 101–108.

(54) Ryckaert, J. P.; Ciccotti, G.; Berendsen, H. J. C. Numerical Integration of the Cartesian Equations of Motion of a System with Constraints: Molecular Dynamics of N-Alkanes. *J. Comput. Phys.* **1977**, *23*, 327–341.

(55) Essmann, U.; Perera, L.; Berkowitz, M. L.; Darden, T.; Lee, H.; Pedersen, L. G. A Smooth Particle Mesh Ewald Method. *J. Chem. Phys.* **1995**, *103*, 8577–8593.

(56) Darden, T.; Perera, L.; Li, L.; Pedersen, L. New Tricks for Modelers from the Crystallography Toolkit: The Particle Mesh Ewald Algorithm and Its Use in Nucleic Acid Simulations. *Structure* **1999**, *7*, R55–R60.

(57) Bussi, G.; Donadio, D.; Parrinello, M. Canonical Sampling through Velocity Rescaling. *J. Chem. Phys.* **2007**, *126*, 014101.